Discontinuous Space-Vector Modulation for Three-Level PWM Rectifiers

Luca Dalessandro, *Member, IEEE*, Simon D. Round, *Senior Member, IEEE*, Uwe Drofenik, *Member, IEEE*, and Johann W. Kolar, *Senior Member, IEEE*

***Abstract*—This paper presents the implementation and experimental verification of two discontinuous pulsewidth modulation (DPWM) methods for three-phase, three-level rectifiers. DPWM's features, such as improved waveform quality, lower switching losses, reduced ac-side passive component size, are investigated and compared to the conventional continuous pulsewidth modulation (CPWM). These features allow higher power density and/or efficiency to be achieved and are important targets for the next generation of power rectifiers. The implementation of the two DPWM strategies is explained by means of space-vectors representation and modulation functions. A detailed analysis of both ac-side and dc-side current waveforms is presented, and there is excellent agreement between the analytical, simulated and experimental results for the mains current ripple amplitude and output center-point current over the practical modulation range. Finally, the control of the center-point voltage is discussed.**

***Index Terms*—Discontinuous pulsewidth modulation, three-phase three-level rectifiers, space-vector modulation.**

I. INTRODUCTION

THREE-PHASE, boost-type, dc-voltage link pulsewidth modulated (PWM) rectifiers have, in general, no connection between the star point N of the supplying mains and the center point M of the output dc voltage (see Fig. 1). Hence, only the differences between the phase voltages formed at the input of the rectifier and the mains voltages have influence on the formation of the mains phase currents. The zero-sequence voltage v_{MN} between M and N can therefore adopt any value and its waveform shape depends on the selected modulation strategy. As consequence, the rectifier input sinusoidal reference voltage can be augmented by a suitably selected zero-sequence voltage to modify the duty-cycle of the rectifier switches and thus implement high-performance modulation strategies [1]–[4].

One modulation method to form sinusoidal currents is by switching only two rectifier phase legs while the third phase leg (where the selected phase changes in a cyclic manner over one mains period) is clamped to an output voltage bus. This can be obtained by using zero-sequence discontinuous-type signals to augment the sinusoidal reference [2], [5]. The method of clamping of a phase leg input voltage to the output bus is called discontinuous pulsewidth modulation (DPWM) and has
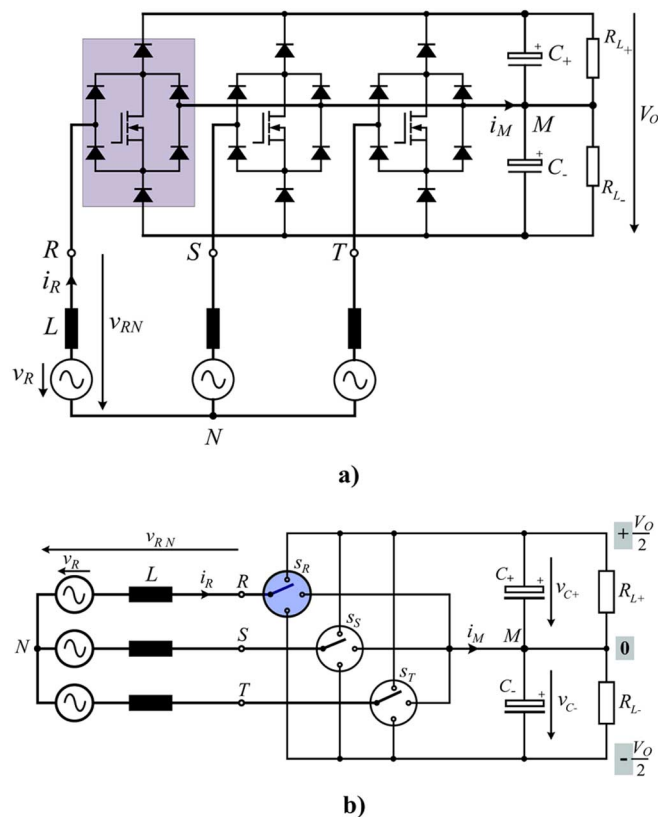
Fig. 1. (a) Power circuit of a three-phase, three-level, *Vienna* rectifier. (b) Simplified model of a three-level rectifier. The clamping of an input rectifier phase-terminal to the positive or negative bus occurs when the switch is off and the input current flows through the upper or lower diodes to the output bus.

reduced switching losses compared to using conventional modulation approaches, where there is constant switching of the power devices, such as in continuous pulsewidth modulation (CPWM) [5]–[8]. For a defined value of allowable switching loss, this allows an increase of the effective switching frequency for DPWM, thus leading to a significant reduction of the rms value of the mains current harmonics for high modulation index values. Additionally, the use of the higher switching frequency results in a reduced filtering effort for the suppression of conducted EMI and the power density of the rectifier system is increased. Continuous and discontinuous PWM methods are typically implemented by using a synchronous-frame voltage-oriented current control scheme based on the space vector concept and this is usually referred as space vector modulation (SVM).

DPWM was first used for three-phase, two-level voltage-source inverters (VSI) [6], [7], [9] in order to reduce the switching losses and improve the efficiency of the converter,

due to the reduced number of device switching instances and the absence of switching in the vicinity of peaks of the phase current [7]. In [5], the analytical derivations of the expression of the modulation signals used to implement the DPWM for two-level VSI are presented. It is shown in [10] that, for the same class of converters, DPWM is superior to CPWM for high values of the modulation index, in terms of linear modulation range, voltage gain, and harmonic distortion. Therefore it is advantageous to swap between different modulation methods according to the modulation index [1]. An improved DPWM method for a two-level VSI used in an active power filter applications is presented in [11], where the modulation method includes an algorithm to predict the peak values of the inverter current and consequently calculate the position of the phase clamping intervals. The advantages of DPWM have been recently verified on multilevel VSI, a class of topologies that offers many benefits for higher power application, such as the ability to synthesize voltage waveforms with lower harmonic content than two-level inverters and operation at higher dc voltages using series connected semiconductor switches. In particular, [3] presents the implementation of DPWM methods for three-level VSIs and [4] investigates the possibility of implementing DPWM strategies for five-level and seven-level VSIs.

Since the main goal of DPWM is to reduce the switching losses, the phase clamping intervals should occur around the peaks of the respective phase current. Therefore, one has to consider the typical current phase lag in ac motor drive VSI applications, where the clamping interval occurs for a phase angle of $60°$ of the fundamental period [7]. In particular, the total clamping interval per phase lasts $120°$ and can be continuous (one phase clamped either to the positive or negative dc rail exclusively) or split up into $2 \times 60°$ and $4 \times 30°$ intervals, using both rails [5], [6]. In [8], DPWM is applied to a two-level PWM rectifier, which operates with a wide power factor range.

This paper investigates and experimentally verifies the application of discontinuous modulation to a three-phase, three-level *Vienna* rectifier [Fig. 1(a)] [12]. The *Vienna* rectifier is a unity power factor (zero phase angle) rectifier with only a unidirectional power flow. Three-level rectifiers have the advantages of lower blocking device voltage and improved quality of the current waveform compared with two-level rectifiers. On the other hand, the balancing of the center point M voltage has to be assured [13]–[15]. Two discontinuous modulation methods can be implemented by eliminating either the first or the last state in the switching sequence, or equivalently, by using only one of the redundant vectors. With this in mind, the analysis presented in this paper shows to what extent the operational behavior of a three-level rectifier, modulated by DPWM, is improved as compared to continuous modulation. This paper's contribution is to present the performance of discontinuous modulated three-level rectifiers from a more practical standpoint, comparing the theoretical analysis with a comprehensive experimental verification using a three switch, three-level *Vienna* rectifier.

In Section II, it is shown how the degree of freedom in the modulation is used to implement the discontinuous schemes. In particular, both a space vector representation and a modulation function are used as a means to explain the two dis-continuous modulation methods introduced in this paper and to clearly show the clamping intervals of the switches. Section III presents a comparison between the two DPWM strategies and CPWM, in terms of mains current ripple and switching losses. Experimental measurements comparing the differences between CPWM and DPWM in terms of the input and center-point current waveforms and relative ripple currents over the practical modulation range are presented in Section IV.

II. DISCONTINUOUS MODULATION SCHEMES

The absence of the neutral current path in three-phase rectifiers provides a degree of freedom in determining the input converter voltage, that constitutes the sinusoidal guidance for the line current according to

$$L\frac{di_i}{dt} = v_i - v_{iN} \quad \text{index } i = R, S, T \tag{1}$$

where v_i and v_{iN} are the mains voltage and the input rectifier voltage for phase-i (referred to the star point N potential), i_i is the phase-i current and L the input inductance. The degree of freedom provided is that the voltage v_{MN} from the center point M and the mains star point N can assume any value. Therefore, zero-sequence signals can be added to the pre-control signal to improve the performance of the modulation [1], [2], [16], and the voltage v_{MN} will be shaped according to the zero-sequence signal injected in the modulator part of the current control loop. The zero-sequence (or common mode) voltage v_{MN} is related to the input rectifier voltage v_{iN} by

$$v_{iN} = v_{iM} - v_{MN} \quad \text{index } i = R, S, T \tag{2}$$

where v_{iM} is the input rectifier voltage referred to the center point M of the dc-link capacitors. Since the input rectifier voltage v_{iN} is defined as a difference according to (2), then its local average value waveform must be sinusoidal in order to generate the required sinusoidal line current. For a current-commutated voltage-source rectifier, like the *Vienna* Rectifier [12] used for the experiments in this work, the generation of the voltage v_{iM} is dependent on the direction of the phase current and is defined as

$$v_{iM} = \begin{cases} \text{sgn}\{i_i\}\frac{V_0}{2}, & \text{if } s_i = \text{sgn}\{i_i\} \\ 0, & \text{if } s_i = 0 \end{cases} \tag{3}$$

where V_0 is the output rectifier voltage (see Fig. 1). According to the value assumed by the phase switching function s_i, the respective input rectifier phase terminal can be clamped to the positive output-voltage rail ($s_i = +$), to the negative rail ($s_i = -$) or to the output center point ($s_i = 0$). For the *Vienna* rectifier, the case when $s_i = 0$ occurs when the power switch is turned on.

In contrast, for a forced-commutated, conventional 6-switch rectifier the switching function $s_i (i = R, S, T)$ is independent of the phase current sign and the input rectifier terminals are clamped to the positive output-voltage rail, the negative one and the center point M only according to the switches status.

A. Space Vectors Representation

All the space vectors available in a mains period for a three-level PWM rectifier are represented in the complex plane as
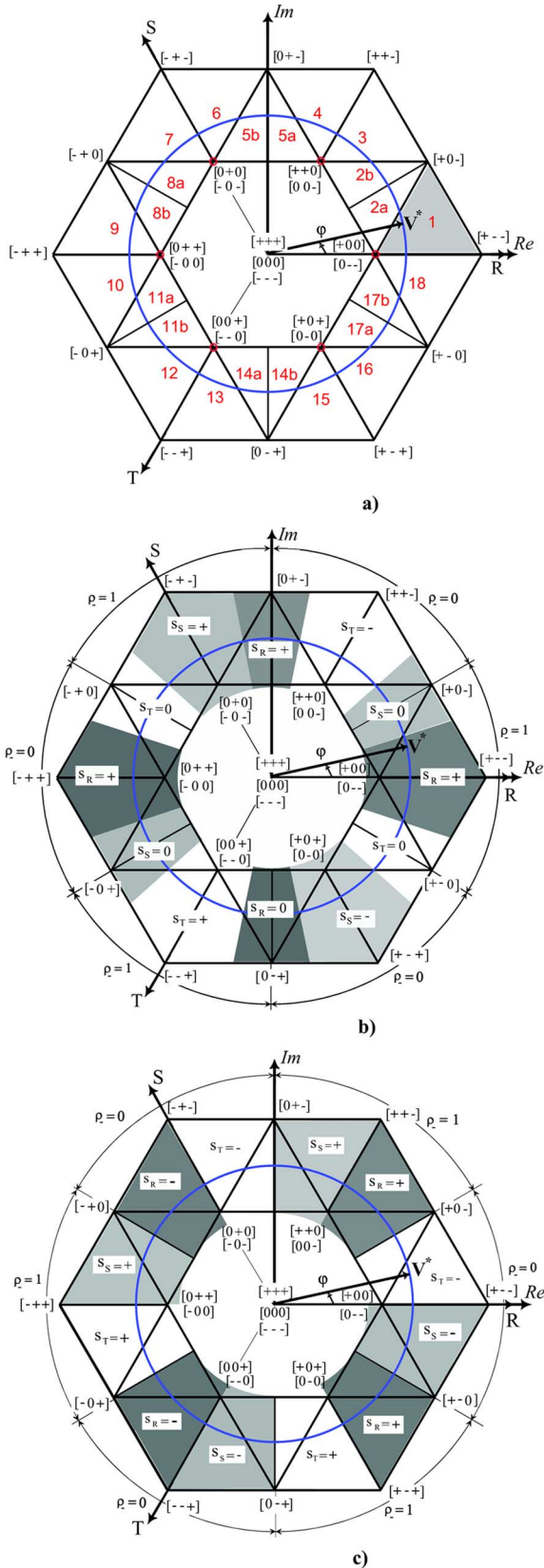
Fig. 2. Switching intervals for: (a) continuous SVM (CPWM); (b) discontinuous SVM method A (DPWMA), characterized by variable intervals, depending on the modulation index M; (c) discontinuous SVM method B (DPWMB) with fixed intervals. The shaded regions in (b) and (c) indicate the clamping intervals of the i-phase, $i = R, S, T$, to the positive rail ($s_i = +$), the negative rail ($s_i = -$), or to the center point ($s_i = 0$). Moreover, the value of the control variable ρ_- (7), either 0 or 1, is indicated as a function of the phase angle φ.

shown in Fig. 2(a). The space vectors are usually classified into zero-voltage vectors, small vectors which are the vertices of the inner hexagon, medium vectors which are midpoints of the sides of outer hexagon, and large vectors comprising of the vertices of the outer hexagon. Each switching state vector is denoted by the triple of quantities (s_R, s_S, s_T) formed by the phase-switching function s_i. The input rectifier reference voltage phasor

$$V^* = \frac{1}{2} M V_0 e^{j\varphi(t)} \tag{4}$$

is formed by averaging the three-nearest available space vectors over a switching period, where M indicates the modulation index, which is defined as

$$M = \frac{\hat{V}_{iN}}{\frac{1}{2} V_0} \tag{5}$$

where $\hat{V}_{iN}$ is the peak value of the rectifier input voltage and $\varphi(t) = 2\pi f t$ is the phase angle dependent on the mains supply frequency f. In this paper, only the interval

$$M \in \left[\frac{2}{3}, \frac{2}{\sqrt{3}} \right] \tag{6}$$

will be considered, which is a typical modulation index range for a practical realization. For example, in a three-phase $400\,V$ line-to-line application the output voltage would be typically limited to $400\,V_{dc}$ since commonly available capacitors have a rated voltage of $450\,V_{dc}$. If the input voltage is considered to range from 320 V to 480 V, then a modulation index from 0.65 to 0.99 would result.

For the current-commutated *Vienna* rectifier, the available space vectors depend on the sign of the phase currents and accordingly, there are eight available space-vectors every 60 degrees [17]. In the direct digital implementation, that uses the space-vectors concept to calculate the duty cycle of the rectifier switches [2], the degree of freedom appears as the partitioning of two redundant switching states. There are six pairs of redundant space-vectors represented by the small vectors in Fig. 2(a). Each pair generates the same line-to-line voltage and this results in a center-point current i_M of same value but the direction of i_M depends on the selected space vector [14]. If δ_- represents the duty-cycle for one pulse period of the redundant switching state that generates a negative i_M (according to the direction indicated in Fig. 1), and δ_+ is the duty-cycle of the space-vector causing positive flowing i_M, then the control parameter that expresses the degree of freedom in the SVM can be defined as:

$$\rho_- = \frac{\delta_-}{\delta_- + \delta_+} \quad \rho_- \in [0, 1] \tag{7}$$

and represents namely the relative on-time of the space-vector producing a negative center-point current i_M. Therefore, the center-point voltage balance can be performed by varying the control parameter ρ_- and it results that the center to neutral point voltage v_{MN} for SVM is shaped according to the modulation strategy implemented and specifically, to the zero-sequence signal added to the pre-control signal or redundant switching vectors selected [14]. The denominator of (7), $\delta_- + \delta_+$, is determined from the modulation of the voltage reference V^*.

In order to minimize the transistors switching, the switching states within each pulse half period can be arranged in such a way that the subsequent state can always be obtained by switching of only one bridge leg [3]. For a three-phase rectifier, using CPWM, the minimum number of switching transitions in one switching period is three, i.e., one for phase leg. The duty cycle of the redundant space vector is split such that the redundant vector occurs at the first and the last position of the switching sequence. To minimize the current ripple, the duty-cycles δ_+ and δ_- are selected to have the same value and this results in ρ_- being equal to 0.5 [4]. Consider sector 1, as shaded in Fig. 2(a) for CPWM, if $(0--)$ is selected, arbitrarily, as the initial switching state, this results within each pulse period T_P a switching state sequence of

$$\cdots|_{t=0}(0--) \rightarrow (+--) \rightarrow (+0-) \rightarrow (+00)|_{t=\frac{1}{2}T_P}$$
$$(+00) \rightarrow (+0-) \rightarrow (+--) \rightarrow (0--)|_{t=T_P}\cdots. \quad (8)$$

It should be noted that the sequence in (8) should be reversed in the next switching period for minimum harmonic impact [4].

The main goal for implementing the discontinuous modulation strategy is to minimize the switching losses; hence the switching of the power transistor has to be preferably avoided around the maxima of the associated phase current. This basic idea, in connection with providing a zero average value of the center-point current within a mains period, results in the discontinuous modulation scheme A (DPWMA), shown in Fig. 2(b). Here, the different colored shaded regions indicate the clamping of a particular phase. For example, in sector 1 where the voltage reference vector V^* is positioned, the input phase R is clamped to the positive bus. This is achieved by turning the power transistor of bridge leg R off, and since the input phase R current is flowing into the rectifier it must flow to the positive output bus, which results in the input rectifier voltage being clamped to the output-voltage positive rail ($s_R = +$). As the phase angle φ advances, in the next phase clamping region the switch in phase S is turned on and phase S is clamped to the center-point voltage ($s_S = 0$).

Discontinuous modulation is implemented by eliminating the first or the last state (corresponding to the redundant vector) in the switching sequence (8), or equivalently by selecting $\rho_- = 0$ or 1. If now $\rho_- = 1$ is set in sector 1 of the space vector plane [see Fig. 2(b)], this results a switching state sequence or DPWMA of

$$\cdots|_{t=0}(\pm00) \rightarrow (\pm0-) \rightarrow (\pm--)|_{t=\frac{1}{2}T_P}$$
$$(\pm--) \rightarrow (\pm0-) \rightarrow (\pm00)|_{t=T_P}\cdots \quad (9)$$

where the input rectifier voltage of phase R is clamped to the output-voltage positive rail ($s_R = +$).

The other discontinuous control scheme (DPWMB), which is independent of the modulation index M, can be obtained by inverting the values of the control parameter ρ_- as compared to DPWMA. The DPWMB clamping intervals, as shown in Fig. 2(c), are now different from DPWMB. If $\rho_- = 0$ is set in sector 1 of the space vector plane [see Fig. 2(c)], this results in the following switching state sequence:

$$\cdots|_{t=0}(0-\underline{-}) \rightarrow (+-\underline{-}) \rightarrow (+0\underline{-})|_{t=\frac{1}{2}T_P}$$
$$(+0\underline{-}) \rightarrow (+-\underline{-}) \rightarrow (0-\underline{-})|_{t=T_P}\cdots. \quad (10)$$

Here, the switch of the phase T is turned off for the complete pulse period and the input rectifier voltage is clamped to the negative output-voltage rail ($s_T = -$). For DPWMB, the clamping takes place in $30°$-wide intervals that are shifted by $\pm45°$ from the maxima of the respective mains phase currents.

B. Modulation Functions

The calculation of the duty cycles of the rectifier switching devices can be determined from the phase modulation functions m_i [18], [19]. For phase i, the equation of the modulation function is expressed as

$$m_i = \frac{v_{iM}}{\frac{1}{2}V_0} = \frac{v_{iN}}{\frac{1}{2}V_0} + \frac{v_{MN}}{\frac{1}{2}V_0}$$
$$= m_i' + m_0 \quad \text{index } i = R, S, T \quad (11)$$

where the sinusoidal reference m_i' is augmented by a zero-sequence waveform, m_0. The signal m_0 and the average value of the neutral point voltage v_{MN} are directly proportional, whereas the average input rectifier voltage v_{iM} can be calculated from (3).

Considering Sector 1 in Fig. 2(a) and using switching pattern and input rectifier voltages given in Appendix A, the modulation functions for the three phases are

$$m_R = \delta_{(+--)} + \delta_{(+0-)} + \delta_{(+00)}$$
$$m_S = -\delta_{(0--)} - \delta_{(+--)}$$
$$m_T = -\delta_{(0--)} - \delta_{(+--)} - \delta_{(+0-)}. \quad (12)$$

The zero-sequence part of the modulation function m_0 is given by

$$m_0 = \frac{1}{3}(m_R + m_S + m_T)$$
$$= -\frac{1}{3}\delta_{(+--)} + \frac{1}{3}\delta_{(+00)} - \frac{2}{3}\delta_{(0--)}$$
$$= -\frac{1}{3}\delta_{(+--)} + \left(\rho_- - \frac{2}{3}\right)(\delta_{(+00)} + \delta_{(0--)}) \quad (13)$$

where the control parameter ρ_-, defined in (7), has the form for Sector 1 of

$$\rho_- = \frac{\delta_{(+00)}}{\delta_{(+00)} + \delta_{(0--)}}. \quad (14)$$

The modulation functions of the sinusoidal references m_i' for each of the three phases can then be determined from (11)–(13) as

$$m_R' = \frac{2}{3}\left(1 + \delta_{(+--)} + \frac{1}{2}\delta_{(+0-)}\right)$$
$$m_S' = -\frac{1}{3}(1 + \delta_{(+--)} - \delta_{(+0-)})$$
$$m_T' = -\frac{1}{3}(1 + \delta_{(+--)} + 2\delta_{(+0-)}). \quad (15)$$

From (13) and (15), it is apparent that a change of ρ_- influences only the zero-sequence part of the modulation function.

Fig. 3 shows the modulation functions of the CPWM, DPWMA and DPWMB for a modulation index $M = 0.815$. For the two discontinuous methods the bridge legs are not switched continuously during one mains period and the clamping intervals of the input rectifier voltage to the positive,
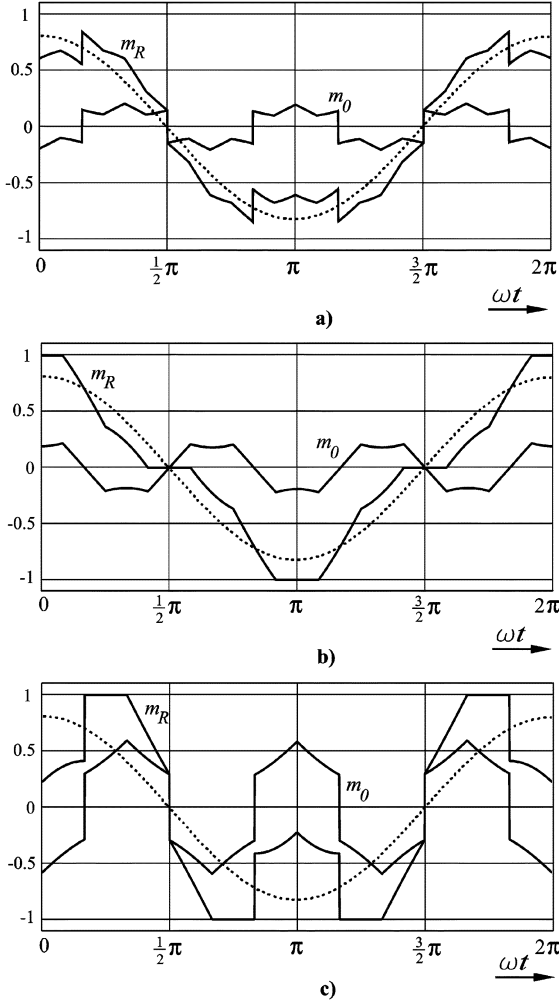
Fig. 3. Modulation functions for the phase R and for modulation index $M = 0.815$. The modulation function m_R (proportional to the average of the input rectifier voltage average value v_{RM}) and its zero-sequence component m_0 (proportional to the average value of v_{MN}) are shown for: (a) CPWM, (b) DPWMA and (c) DPWMB.

negative, and center-point, characteristic of the discontinuous modulation are apparent from Fig. 3. Note that for the DPWMA there are clamping intervals during the phase current zero-crossings and this is an advantage as the generation of the modulation waveforms is not dependent on accurately determining the mains phase-voltage zero crossing.

III. COMPARISON OF CONTINUOUS AND DISCONTINUOUS MODULATION SCHEMES

A. Normalization

In order to obtain an independency of the simulations and experiments from the selected specific parameters and to derive results which are not limited to specific operating parameters and device characteristics, the calculated average and rms current values are related to the peak value $\hat{I}^*$ of the mains current reference value. The normalized rms value of the power transistor current is then

$$I_{\mathrm{rms},r} = \frac{I_{\mathrm{rms}}}{\hat{I}^*}. \qquad (16)$$

The normalization basis of the rms value of the mains current ripple ΔI_{rms} is set to

$$\Delta I_r = \frac{V_0 T_P}{8L}. \qquad (17)$$

Thus

$$\Delta I_{\mathrm{rms},r} = \frac{\Delta I_{\mathrm{rms}}}{\Delta I_r} \qquad (18)$$

and represents a characteristic value which is independent from the switching frequency f_P and the input inductance value L in a first approximation. The subscript r represents a normalized parameter.

B. Calculation of Switching Frequency Increase

The admissible increase of the switching frequency for equal thermal stress on the switches is now calculated. As shown in [12] the global (over a mains period) switching losses of the transistor of a *Vienna* Rectifier phase leg can be calculated by averaging the local switching losses $p_T = (1/T_P) w_P$ according to

$$P_T = \frac{1}{\frac{\pi}{2}} \int_0^{\frac{\pi}{2}} p_T \, \mathrm{d}\varphi \qquad (19)$$

where the integration can be limited to $(1/4)T_N$ or $(\pi/2)$ due to symmetry reasons and T_N is the mains period. The switching loss w_P within one pulse period T_P, given by the sum of the turn-on loss and the turn-off loss, can be expressed as a linear function the switched phase current

$$w_P = k_f \, i \qquad (20)$$

where k_f is a constant dependent on the voltage across the switch and the switch characteristics and i indicates the phase current.

Assuming for CPWM a purely sinusoidal shape of the switched current (see Appendix C), it follows

$$P_{T,\mathrm{CPWM}} = \frac{2}{\pi} k_f \hat{I} f_P \qquad (21)$$

where $\hat{I}$ is the peak value of the phase currents and f_P the pulse frequency.

For discontinuous modulation, the clamping intervals shown in Fig. 3(b) and (c) have to be omitted from the integration (19). Since the integration interval for DPWMA is dependent on the modulation index M, then also the resulting switching losses $P_{T,DPWMA}$ show a dependency on the modulation index M as given by

$$P_{T,DPWMA} = \frac{2}{\pi} \frac{1}{\sqrt{3}M} k_f \hat{I} f_P. \qquad (22)$$

Close to the overmodulation limit, $M = M_{\mathrm{max}}$ (6), the switching losses (22) are reduced by factor of 2 as compared to continuous modulation, and for $M = (2/3)$ there is a reduction by a factor of $(\sqrt{3}/2)$.

As shown in [6], the conduction losses are in good approximation independent of the modulation scheme (continuous or discontinuous modulation). Therefore, under the assumption of equal thermal stress of the power transistors as in continuous
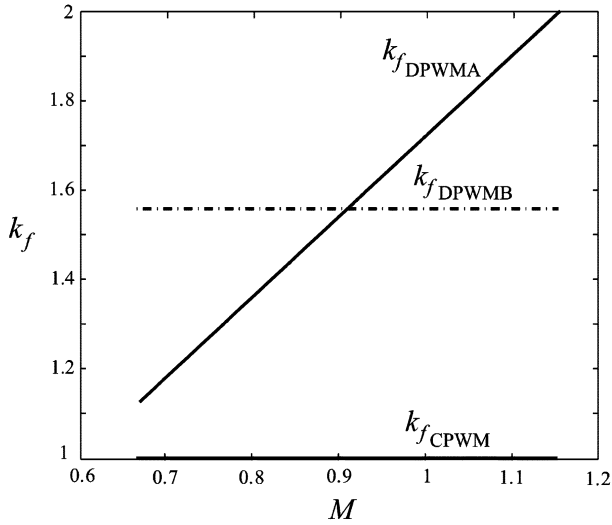
Fig. 4. Factors k_f as a function of the modulation index M, indicating the increase of switching frequency for a) DPWMA ($k_{f,DPWMA}$) and b) DPWMB ($k_{f,DPWMB}$), with respect to c) CPWM ($k_{f,CPWM}$).

Fig. 5. Representation of the impact of the redundant switching states distribution on the mains current ripple Δi_R over a pulse period T_P. The duty cycles δ_- and δ_+ of the redundant space vectors are expressed as a function of the control parameter ρ_- (7).

Fig. 6. Analytical (solid lines), simulated (dashed lines), and experimental (marked points) results showing the dependency of the square of the rms value of the phase current ripple on the modulation index M for (a) DPWMA, (b) DPWMB, and (c) CPWM.

modulation (21), the switching frequency of DPWMA can be increased by a factor of

$$k_{f,\text{DPWMA}} = \sqrt{3}M \qquad (23)$$

A similar consideration shows for DPWMB the possibility of increasing the switching frequency by a constant factor of

$$k_{f,DPWMB} = \frac{2}{3 - \sqrt{3}} \approx 1.58. \qquad (24)$$

In contrast to the DPWMA, there is no dependency of k_f on M for DPWMB (see Fig. 4). This can be explained by the independency of the relative duration and position of the clamping intervals of M for DPWMB.

C. Impact of the Redundant Switching States Distribution on ac-Side Currents

As compared to continuous modulation, discontinuous modulation has in general a lower ripple of the mains phase current due to the higher effective switching frequency. Besides the switching frequency, the ripple of the mains phase current is also influenced by the distribution of the redundant switching states between the beginning and end of one pulse half period as illustrated in Fig. 5. As shown in [4], the rms value of the mains current ripple can be minimized for continuous modulation by defining $\rho_- \approx 0.5$ in wide intervals of the mains period. Therefore, for discontinuous modulation, characterized by values of the control parameter $\rho_- = 0$ or 1 [see Fig. 2(a)], an increase in the current ripple has to be expected. However, there is a reduction in the ripple through the increasing of the switching frequency by a factor k_f, (23)–(24).

The normalized mains current ripple can be calculated analytically for the continuous and discontinuous modulation methods by determining the equations of the squared and normalized current sum averaged over the switching period
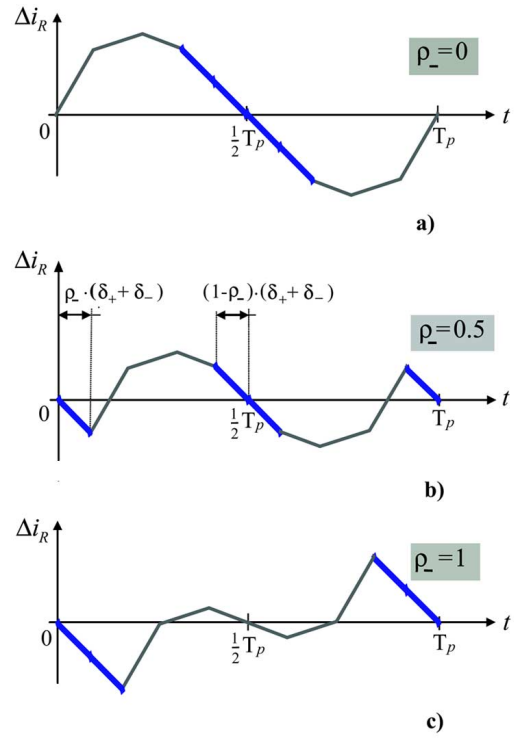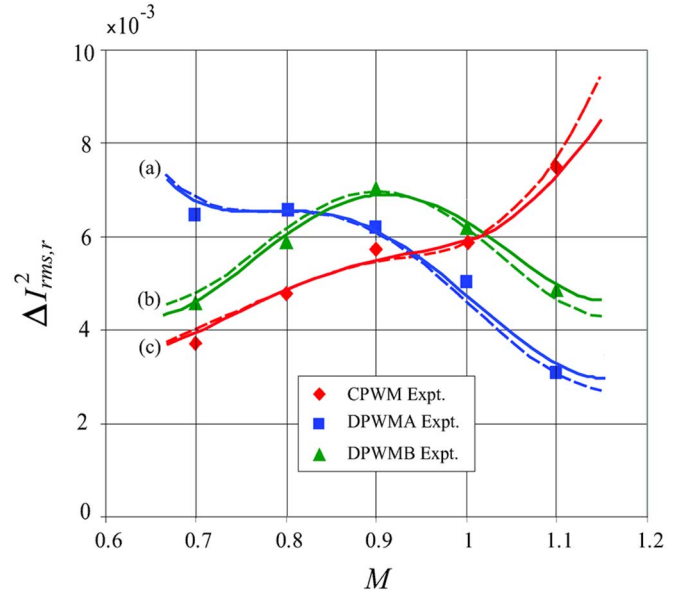
for each sector. Appendix B describes the basis for this calculation. The analytical equations for the squared current ripple of CPWM, DPWMA and DPWMB are given in (25)–(27), respectively. The results from these equations are plotted over the practical modulation index range in Fig. 6, where they are
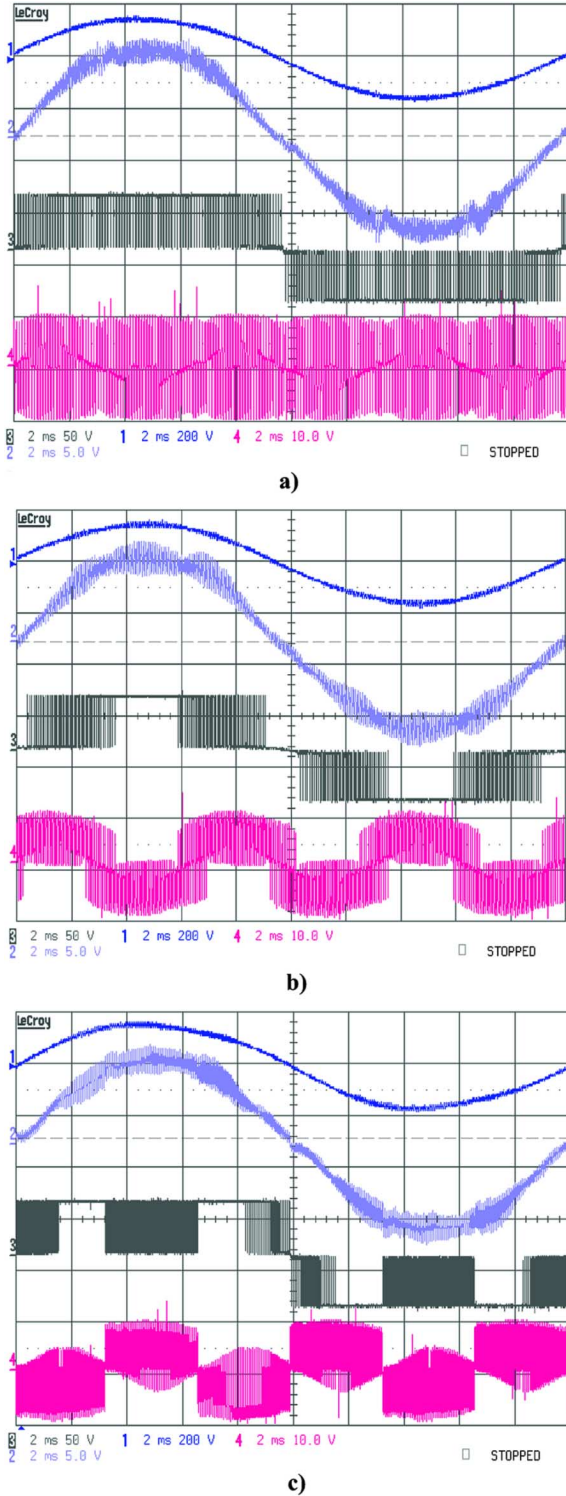
Fig. 7. Experimental waveforms recorded for: (a) CPWM, (b) DPWMA, and (c) DPWMB. The modulation index is $\mathrm{M} = 0.9$. Ch1: mains voltage (200 V/div). Ch2: mains current (5 A/div). Ch3: input rectifier voltage (200 V/div). Ch4: neutral point current i_M (10 A/div). Time base 2 ms/div.

compared with simulation and experimental results. It can be seen that at lower modulation indexes the current ripple for CPWM is lower than both the DPWM schemes, however for

$M > 0.95$ DPWMA starts to have a much lower current ripple than CPWM

$$\Delta I^2_{rms,r,\mathrm{CPWM}}$$
$$= \left[\frac{2\pi - 3\sqrt{3}}{9\pi} + \frac{4}{9\pi} arcsin \left(\frac{1}{\sqrt{3}\,M} \right) \right]$$
$$+ M \cdot \left(-\frac{4}{\pi} + \frac{22}{9\sqrt{3}\,\pi} \sqrt{1 - \frac{1}{3M^2}} \right)$$
$$+ M^2 \cdot \left[\frac{2}{\pi} arcsin \left(\frac{1}{\sqrt{3}\,M} \right) + \frac{3\pi - \sqrt{3}}{2\pi} \right]$$
$$+ M^3 \cdot \left(\frac{-72 + 16\sqrt{3}}{9\pi} + \frac{8}{3\sqrt{3}\,\pi} \sqrt{1 - \frac{1}{3M^2}} \right)$$
$$+ M^4 \cdot \left(\frac{3\pi - 3\sqrt{3}}{4\pi} \right) \tag{25}$$

$$\Delta I^2_{rms,r,\mathrm{DPWMA}}$$
$$= \frac{1}{3M^2} \left\{ \frac{20}{9} \right.$$
$$+ \frac{2}{\pi} \left[\sqrt{3} - \frac{28}{9} \arcsin \left(\frac{1}{\sqrt{3}M} \right) \right]$$
$$- \frac{308}{9\sqrt{3}\,\pi} M \sqrt{1 - \frac{1}{3M^2}}$$
$$+ M^2 \left[13 + \frac{5\sqrt{3}}{\pi} - \frac{34}{\pi} \arcsin \left(\frac{1}{\sqrt{3}M} \right) \right]$$
$$- \frac{2}{3\sqrt{3}\,\pi} M^3 \left(4 + 83 \sqrt{1 - \frac{1}{3M^2}} \right)$$
$$\left. + \frac{3}{2} M^4 \left(1 + \frac{3\sqrt{3}}{2\pi} \right) \right\} \tag{26}$$

$$\Delta I^2_{rms,r,\mathrm{DPWMB}}$$
$$= \frac{(3 - \sqrt{3})^2}{4} \left\{ \left[\frac{4}{3} - \frac{8}{9\pi} arcsin \left(\frac{1}{\sqrt{3}\,M} \right) \right] \right.$$
$$- M \cdot \left[\frac{12 + 16\sqrt{3}}{3\pi} + \frac{44}{9\sqrt{3}\,\pi} \sqrt{1 - \frac{1}{3M^2}} \right]$$
$$+ M^2 \cdot \left[-\frac{4}{\pi} arcsin \left(\frac{1}{\sqrt{3}\,M} \right) + \frac{17\pi + 21\sqrt{3}}{3\pi} \right]$$
$$- M^3 \cdot \left[\frac{-9 + 104\sqrt{3}}{9\pi} + \frac{16}{3\sqrt{3}\,\pi} \sqrt{1 - \frac{1}{3M^2}} \right]$$
$$\left. + M^4 \cdot \left[\frac{6\pi + 3\sqrt{3}}{4\pi} \right] \right\}. \tag{27}$$

D. Impact of the Redundant Switching States Distribution on the Center Point Current

The implementation of discontinuous modulation schemes by setting the control parameter ρ_- equal to 1 (DPWMA) or 0 (DPWMB) also has a direct influence on the shape of the

center-point current i_M through the shape of the neutral point voltage v_{MN}. The center-point current i_M is dependent on the phase currents according to

$$i_M = t_R i_R + t_S i_S + t_T i_T, \qquad t_i = \begin{cases} 1, & \text{if } s_i = 0 \\ 0, & \text{else} \end{cases} \quad (28)$$

where the function t_i (index $i = R, S, T$) is unitary only when the phase input terminal is clamped to the center point. In [14], it is clearly shown that only short (redundant) and average vectors contribute to the center-point current. Redundant switching states result in center-point current i_M of same value but different sign. In particular, for sector 1 in Fig. 2(a), the center-point current corresponding to the redundant switching states $(0 - -)$ and $(+00)$ is calculated as

$$i_M = \begin{cases} -i_R, & \text{for } (0 - -) \\ +i_R, & \text{for } (+00) \end{cases} \quad (29)$$

while the local average within the half-pulse period in the same sector is given by

$$i_{M,\text{avg}} = (\delta_{(0--)} - \delta_{(+00)}) i_R + \delta_{(+0-)} i_S. \quad (30)$$

Since ρ_- (14) alternates between 0 and 1 six times the mains frequency (see Fig. 2), and from (28) and (30), a relative high amplitude of the third harmonic in the center-point current waveform has to be expected.

IV. EXPERIMENTAL VERIFICATION

The continuous and the two discontinuous modulation schemes are experimentally evaluated using a 5-kW, 115-V, three-level *Vienna* rectifier. The current control, modulation, and switch signals are implemented digitally using an Analog Devices ADSP21992 160 MHz DSP. The line currents and output voltages are sampled at the switching frequency and are used by the dc output voltage and current controllers to generate the duty cycles for the PWM generator. The modulation strategies are implemented in the DSP using a synchronous-frame voltage-oriented current control scheme. The voltage-oriented control for a unity power-factor only requires the control of the synchronous d-component of the current phasor. Inaccurate detection of the phase current zero-crossings can result in additional low frequency distortion when using conventional modulation, however with DPWMA, one phase is clamped during the zero-crossing and therefore does cause any additional distortion.

To complement the experimental results, the three modulation schemes have been simulated using Simplorer for different modulation index values using the same experimental parameters as listed in Table I. The switching frequency for continuous modulation is set equal to 10 kHz, whereas for the discontinuous schemes the coefficients (23) and (24) are considered since equal switching losses are assumed as the basis for the comparison. In particular, the switching frequency for the DPWMA is dependent on the modulation index and it assumes the maximum value for $M = (2/\sqrt{3})$.

In order to evaluate the waveform quality over the whole modulation range, the line and center-point current, and input

TABLE I
EXPERIMENTAL SETUP PARAMETERS

parameter	symbol	value
mains voltage	v_{rms}	115 V
output voltage	V_0	350 V
rms line current	I	6 A
switching frequency	f_P	10 kHz
input inductance	L	500 μH

rectifier voltage (v_{iM}) have been recorded for the three modulation strategies (CPWM, DPWMA, and DPWMB) and for five discrete values of the modulation index. The variation of the modulation index (6) is obtained by keeping the output voltage V_0 constant while changing the supply voltage amplitude. As an example, a set of waveforms are shown in Fig. 7 for a modulation index $M = 0.9$ and for each modulation scheme. Here the phase and the center-point currents are seen in channels 2 and 4 and the input rectifier voltage (3) in channel 3 where the clamping intervals characteristic of discontinuous modulation are apparent in Fig. 7(b) and 7(c).

Fig. 8 shows the input current ripple waveform and frequency spectrum for modulation depth $M = 0.7$ normalized by the fundamental component. The switching frequency for the discontinuous schemes is calculated according to the coefficients (23) and (24). The harmonic components of the mains current, which are grouped around multiples of the switching frequency are shifted to higher frequencies for both discontinuous schemes and this is advantageous in dimensioning of the input EMI filter. In particular for DPWMA, the relative position of the harmonic components in the frequency spectrum is dependent on the modulation index M in order to produce the same switching loss. The frequency spectrum of the DPWMB is independent on the modulation index and the relative position of the harmonic components with respect to continuous modulation is always as shown in Fig. 8.

A conventional criteria to evaluate the waveform quality of different modulation schemes is the the square rms value of the current ripple [6]. The comparative evaluation of the current ripple for the three modulation strategies, normalized according to (16)–(18), is shown in Fig. 6. The results from experimental measurements show a very good correspondence to the analytical equations and simulation results shown as solid and dashed lines, respectively.

If the rectifier is operated close to the overmodulation limit in case of DPWMA, then the harmonic losses are reduced by a factor of ≈ 3 with respect to CPWM (the rms value of the mains current harmonics is then reduced by a factor of $\sqrt{3}$). The use of DPWMB results in a reduction of the switching losses by factor 2 (the rms value of the mains current harmonics is then reduced by a factor of $\sqrt{2}$). For practical realization, therefore, DPWMA has to be preferred to DPWMB although the calculation effort for DPWMA is higher due to the dependency of the clamping intervals on the modulation index M. The results are also in general agreement with the comparative evaluations carried out for continuous and discontinuous modulation schemes of two-level converters [1], [5], [6].

According to (14) and (30), the maximum negative and the maximum positive local average value $i_{M,\text{avg}}$ of the center-point current occurs during one pulse period for $\rho_- = 0$ and
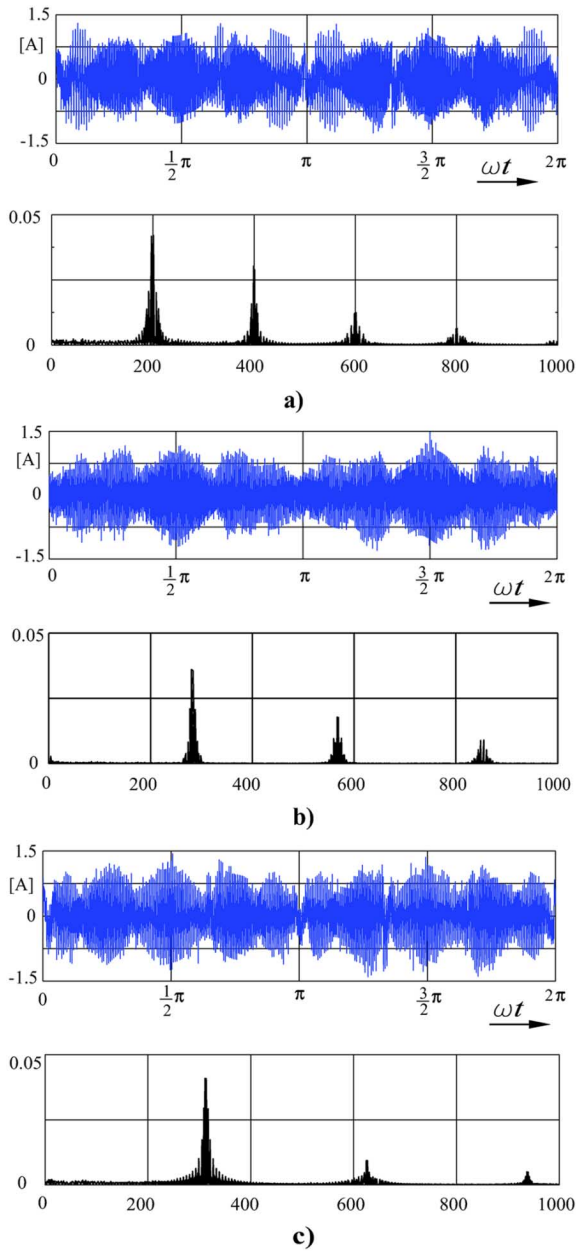
Fig. 8. Measured input current ripple waveform and frequency spectrum for: (a) CPWM, (b) DPWMA, and (c) DPWMB. The modulation index is $M = 0.7$ and the amplitudes are normalized by the fundamental component of the current $(6\,\mathrm{A}_{rms})$, while the frequency components are multiples of the mains frequency (50 Hz).

Fig. 9. Experimental neutral point current harmonic components $I_{M(n)}$ normalized by the fundamental component of the mains current $(6\,\mathrm{A}_{rms})$ and multiples of the mains frequency (50 Hz) for modulation index $M = 0.8$. (a) CPWM, (b) DPWMA, and (c) DPWMB.

Fig. 10. Experimental and simulated results showing the dependency of the normalized amplitude $I_{M(3)}$ of the third harmonic of the center-point current on the modulation index M for (a) CPWM, (b) DPWMA, and (c) DPWMB.

$\rho_- = 1$, respectively. The switching of ρ_- between 0 and 1 with three times the mains frequency (see Fig. 2), which is characteristic for discontinuous modulation, results in a relatively high amplitude of the third harmonic of the center-point current (see Fig. 9). In contrast, for optimized continuous modulation (characterized by $\rho_- \approx 0.5$) there is on average a cancellation of the positive and negative portion of i_M within one pulse period. Therefore, the low-frequency harmonics $\hat{I}_{M,(n)}(n = 3, 9, 15, \ldots)$ of i_M show relatively low amplitudes. In order to limit to a given maximum value the potential shift of the center point caused by the low-frequency harmonics $\hat{I}_{M,(n)}$ of the center-point current, a higher output capacitor value has to be used for discontinuous modulation.
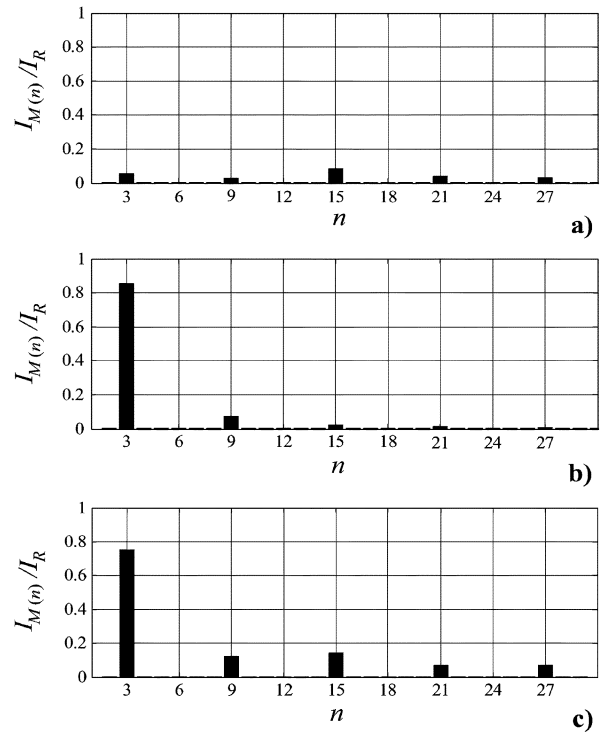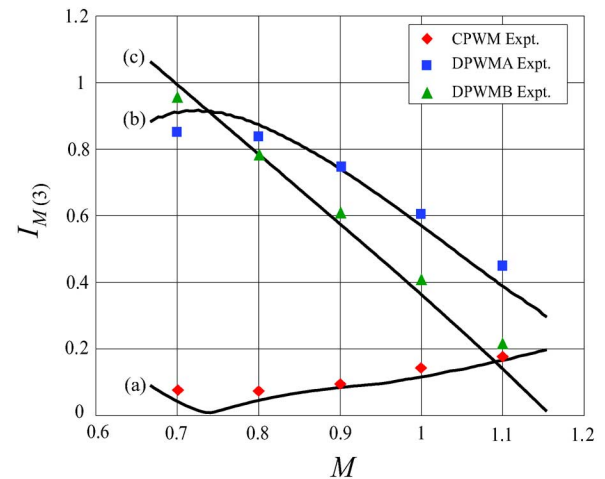
As shown in Fig. 10 for DPWMA there is an approximately linear decline of the amplitude of the third harmonic of the center-point current for increasing modulation index M. This can be explained by the decreasing value of the sum of the redundant switching states durations (7), which is also linear with M and which results in a proportional reduction of the local average value and amplitude of the low-frequency harmonics of the center-point current. For a high modulation index, the base for calculating the necessary output capacitance (using electrolytic capacitors) is therefore is the rms value of the capacitor current $I_{C,rms}$ rather than the above described potential shift of the center point.

In contrast to the low-frequency harmonics of i_M, the rms value of the output capacitor current is *not* influenced by the control parameter ρ_- for balanced partial output voltages and can, therefore, be derived (see Appendix D) for CPWM ($\rho_- = 0.5$), DPWMA, and DPWMB as

$$I_{C,\mathrm{rms},r}^2 = \frac{10\sqrt{3}M}{8\pi} - \frac{9M^2}{16}. \tag{31}$$

For the redundant switching states, the center-point current shows different signs but equal absolute value (28). Therefore, the rms value of the current being fed into the capacitive center point M and being distributed between the both output capacitors equally and/or the output capacitor rms value are independent of ρ_-.

V. DISCUSSION

The control of the center-point voltage should be implemented and has been addressed in several publications [3], [13]–[15]. Although the partial dc-link output voltages are balanced over one mains period for both continuous and discontinuous modulations under ideal conditions, the main task is to maintain long-term stability for higher modulation depth (where the relative duty-cycle of the redundant switching states becomes smaller) and/or in case of unbalanced, nonlinear loads or no-load operation. The center-point balancing control strategies are based on the same degree of freedom used to implement the current control, and specifically on the addition of a zero-sequence component to the sinusoidal [13] and on adjusting the redundant switching sequences [14]. These approaches would introduce further switching transitions and deteriorate the harmonic performance of the modulation as discussed in [3]. A center-point balancing control strategy based on variation of the input current amplitudes rather than the use of redundant switching states is proposed in [15] and its performance with no-load or low-load operation is demonstrated. This control strategy could be combined with a discontinuous modulation scheme, at the expense of line current harmonic distortion; nevertheless the suppression of low frequency ripple of the center-point current and/or additional phase current harmonics represent a minor issue for which other conventional balancing strategies can be applied [3], [15].

The main advantage of discontinuous modulation as compared to continuous modulation is the possibility of increasing the effective switching frequency. The reduction of the rms value of the mains current ripple is then a consequence. If the EMI-filter (which has to be provided at the input side of the rectifier for a practical realization) size is set as basis for the comparison among the modulation schemes, then for a second order filter with a cut-off frequency considerably lower than the switching frequency, the doubling of the switching frequency will result in an increase of the attenuation by a factor of 4. This increase in attenuation is by far more effective than the reduction of the rms value of the mains current ripple due to the increase of the effective switching frequency (factor $\approx \sqrt{3}$). If the rms value of the mains current ripple is thought to be concentrated in a single harmonic with effective switching frequency, the total improvement of the damping of mains current harmonics caused by discontinuous modulation results to a factor of $\approx 4\sqrt{3} \approx 7$.

As is shown in Fig. 10, both DPWM methods have a larger third harmonic center-point current, which is more significant at lower modulation indices, than CPWM. This current flows into the parallel connection of the output capacitors (with an effective value of $2C$). Therefore, to maintain the same level of third harmonic voltage ripple, as in CPWM, would require an increase of output capacitance value, especially at low values of M. This would result in a decrease of the power density of the rectifier. However, in a practical three-phase rectifier application there is the requirement of a defined hold-up time and/or operation under a phase-loss condition. When operating with only two phases, the output capacitors now have a significant second harmonic current flowing in the series connected output capacitors (with effective value of $C/2$). Overall, the required value of the capacitors for the hold-up and/or phase-loss requirements dominates over the increase in capacitor value due to increased third harmonic current of the DPWM methods at low values of M. Therefore, in a practical *Vienna* Rectifier implementation the use of DPWM compared to CPWM would not change the power density when only the output capacitors are considered.

VI. CONCLUSION

This paper has investigated the application of discontinuous modulation schemes for three-level rectifiers. Based on the knowledge of discontinuous PWM as implemented for two-level converters, a theoretical and experimental analysis of two discontinuous PWM methods are compared with continuous PWM. The main advantage of the discontinuous modulation implemented for three-level rectifiers is the possibility of increasing the switching frequency, which allows the reduction of the input current ripple as well as a considerable reduction in the input EMI filter size. The switching losses are also lower compared to continuous modulation.

The presented DPWMA has demonstrated to have better performance than DPWMB and CPWM, especially for high modulation indices ($M > 0.93$). However, it is shown that discontinuous modulation results in a dominant third harmonic in the center-point current and the implementation of the center-point voltage control may introduce further switching transitions, hence resulting in a poorer harmonic performance of the modulation.

For practical realization of the current control of three-level rectifier, discontinuous modulation is preferred to continuous modulation, especially if high power density and/or low filtering effort and/or small size of the ac-side passive components are required. Since the advantages of the discontinuous modulation are recognized for higher modulation indices, it may be a good strategy to swap between different modulation strategies according to the rectifier's operating point, thus realizing a high-performance adaptive modulation algorithm [1], [3].

APPENDIX

A. Switch Signals and Input Rectifier Voltage for Sector 1

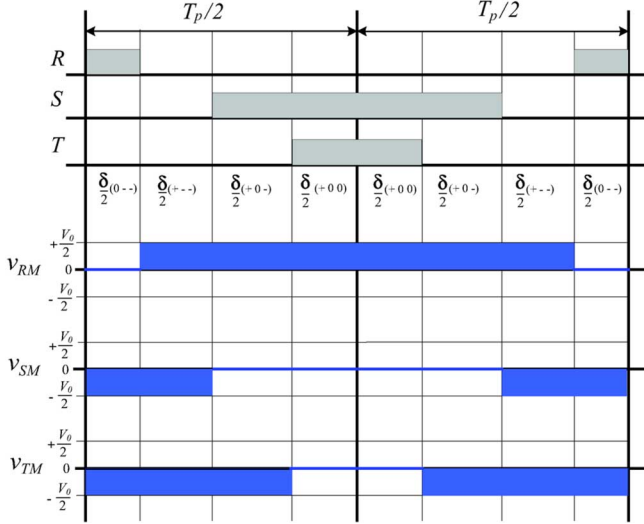Fig. 11 shows the switch gate signals of the *Vienna* rectifier for the first sector.

Fig. 11. *Vienna* rectifier switch gate signals and rectifier input voltages for one switching period T_P in the first sector.
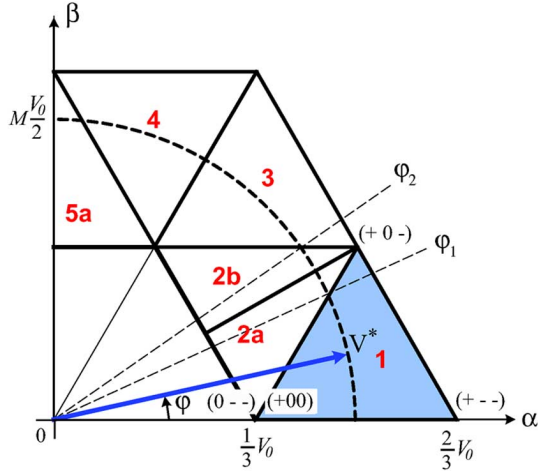

Fig. 12. Representation of the M dependent border angles φ_1 and φ_2 between two sectors and, in particular, of the space vectors available in sector 1.

From the switching pattern and the duty cycles of the applied vectors, the input rectifier to center-point voltages are shown and are given by

$$v_{RM} = \frac{1}{2}V_o(1 - \delta_{(0--)})$$

$$v_{SM} = -\frac{1}{2}V_o(\delta_{(0--)} + \delta_{(+--)})$$

$$v_{TM} = -\frac{1}{2}V_o(1 - \delta_{(+00)}). \tag{32}$$

B. Space Vectors Duty Cycle Calculation for Sector 1

The sector border angles φ_1 and φ_2 shown in Fig. 12 are dependent on the modulation index M and defined as

$$\varphi_1 = \frac{\pi}{3} - \varphi_2$$

$$\varphi_2 = \arcsin \frac{1}{\sqrt{3}M}. \tag{33}$$

The voltage reference phasor V^* is given by the time average over one switching period T_p of the space vectors available in Sector 1

$$V^*(\varphi) = \delta_{(0--)}v_{(0--)} + \delta_{(+--)}v_{(+--)}$$
$$+ \delta_{(+0-)}v_{(+0-)} + \delta_{(+00)}v_{(+00)} \tag{34}$$

where in the first sector the space vectors are, respectively

$$v_{(0--)} \equiv v_{(+00)} = \frac{1}{3}V_0$$

$$v_{(+--)} = \frac{2}{3}V_0$$

$$v_{(+0-)} = \frac{1}{\sqrt{3}}V_0 e^{j\frac{\pi}{6}} \tag{35}$$

and the duty cycles in a switching period T_P add up to unity

$$1 = \delta_{(0--)} + \delta_{(+--)} + \delta_{(+0-)} + \delta_{(+00)}. \tag{36}$$

A complex modulation index is defined as

$$\frac{V^*}{\frac{1}{2}V_0} = m_\alpha + jm_\beta. \tag{37}$$

By replacing (35) in (36) and considering (36) and (37), it follows that the real and imaginary parts of the complex modulation function are given respectively by:

$$m_\alpha = 1 + \frac{1}{3}\delta_{(+--)} - \frac{1}{3}\delta_\rho \tag{38}$$

$$m_\beta = \frac{1}{\sqrt{3}}\delta_{(+0-)} \tag{39}$$

where $\delta_\rho = \delta_{(0--)} + \delta_{(+00)}$. Hence, the space vectors duty cycle for the Sector 1 can be expressed as a function of the modulation index as

$$\begin{pmatrix} \delta_\rho \\ \delta_{(+--)} \\ \delta_{(+0-)} \end{pmatrix} = \begin{pmatrix} 2 & -1 & -1 \\ -1 & 1 & -1 \\ 0 & 0 & -2 \end{pmatrix} \tilde{m} \tag{40}$$

where

$$\tilde{m} = \begin{pmatrix} 1 \\ \frac{3}{2}m_\alpha \\ \frac{\sqrt{3}}{2}m_\beta \end{pmatrix} = \begin{pmatrix} 1 \\ \frac{3}{2}M\cos\varphi \\ \frac{\sqrt{3}}{2}M\sin\varphi \end{pmatrix}. \tag{41}$$

The expression of the duty cycles as a function of the modulation index, exemplarily shown for the first sector, is the basis for the calculation of the current ripple (25)–(27) as well as of the capacitor current (31), calculated in Appendix D.

C. Switching Loss Calculation

Assuming sinusoidal mains currents, the switching losses are defined as

$$P_T = \frac{1}{\pi} \int_0^\pi f_P k_f |i(\varphi)| d\varphi. \tag{42}$$

For CPWM, with $\rho = 0.5$, the switching occurs continuously over the entire fundamental period $[0, 2\pi]$. The product $k_f|i(\varphi)|$ relevant for the switching losses in CPWM is plotted in Fig. 13(a) for the phase R and is normalized by $k_f f_P \hat{I}$. The losses can be calculated integrating the function $k_f|i(\varphi)|$ according to (42) and setting the appropriate integration intervals, resulting in (21).
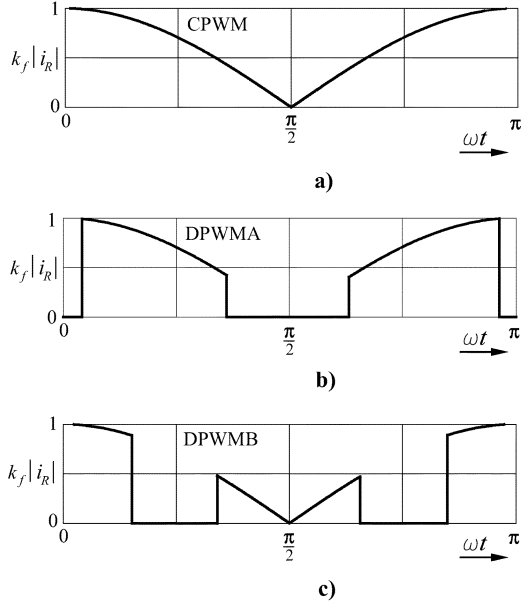
Fig. 13. Normalized functions $k_f|i(\varphi)|$ relevant for the calculation of the switching losses represented over half mains period for (a) CPWM, (b) DPWMA, and (c) DPWMB. The function $k_f|i(\varphi)|$ for DPWMA is represented for $M = 0.8$ and the clamping intervals are dependent on M according to (33).

Observe that for DPWMA the phase switches are clamped over defined intervals, hence the switching losses are zero and therefore $k_f = 0$. The resulting product $k_f|i(\varphi)|$ is shown in Fig. 13(b) for DPWMA and $M = 0.8$. For DPWMA the section angles (33) defining the clamping intervals are dependent on M (see Fig. 2).

For DPWMB, the clamping intervals are different than DPWMA and independent of M. The function $k_f|i(\varphi)|$ for DPWMB is shown in Fig. 13(c). Therefore contrary of DPWMA, the factor of possible frequency increase for DPWMB is M-independent (23)–(24).

D. Output Capacitors RMS Current

The average value over a switching period of the current $i_{+,avg}$ in the positive bus bar within the interval $[0, (\pi/3)]$ can be defined as a function of ρ (14) and for Sectors 1, 2a, 2b, and 3 as follows:

$$
\begin{aligned}
i_{+,avg,1}(\varphi) &= (\delta_{(+--)} + \delta_{(+0-)} + \rho(\delta_{(+00)} + \delta_{(0--)}))i_R \\
i_{+,avg,2a}(\varphi) &= (\delta_{(+0-)} + \rho\delta_{(+00)} + \delta_{(0--)})i_R \\
i_{+,avg,2b}(\varphi) &= (\delta_{(+0-)} + \delta_{(0--)})i_R \\
&\quad + \rho(\delta_{(++0)} + \delta_{(00-)})(i_R + i_S) \\
i_{+,avg,3}(\varphi) &= \delta_{(+0-)}i_R \\
&\quad + (\delta_{(++-)} + \rho(\delta_{(++0)} + \delta_{(00-)}))(i_R + i_S)
\end{aligned}
\tag{43}
$$

where the method to calculate the space vectors duty cycles is shown in Appendix B. The integration of the currents (43) gives

the global average the current in the positive bus bar. If the distribution ρ is set according to the DPWMA scheme, then

$$
\begin{aligned}
I_{+,avg,DPWMA} = \frac{1}{\frac{\pi}{3}} \Bigg(&\int_0^{\varphi_1} |i_{+,avg,1}(\varphi)|_{\rho=1} d\varphi \\
&+ \int_{\varphi_1}^{\frac{\pi}{6}} |i_{+,avg,2a}(\varphi)|_{\rho=1} d\varphi \\
&+ \int_{\frac{\pi}{6}}^{\varphi_2} |i_{+,avg,2b}(\varphi_N)|_{\rho=0} d\varphi \\
&+ \int_{\varphi_2}^{\frac{\pi}{3}} |i_{+,avg,3}(\varphi)|_{\rho=0} d\varphi \Bigg)
\end{aligned}
\tag{44}
$$

where φ_1 and φ_2 are defined as shown in Fig. 12. In order to calculate the rms-value of the positive bus bar current, the squared values of the currents have to be considered in (43) averaged over the switching period. The squared current can be written for each sector in a general form analogous to (43), and integrated similar to (44) referring to the integration intervals for DPWMA.

Finally, the rms-current into the upper output capacitor (C_+ in Fig. 1) can be calculated as

$$
I_{C,rms}^2 = I_{+,rms}^2 - I_{+,avg}^2
\tag{45}
$$

and this leads to (31), which is a result independent of the modulation scheme.

REFERENCES

[1] A. M. Hava, R. J. Kerkman, and T. A. Lipo, "A high-performance generalized discontinuous PWM algorithm," *IEEE Trans. Ind. Appl.*, vol. 34, no. 5, pp. 1059–1071, Sep./Oct. 1998.

[2] C. B. Jacobina, A. M. Lima, and E. R. da Silva, "Digital scalar pulse-width modulation: A simple approach to introduce non-sinusoidal modulating waveforms," *IEEE Trans. Power Electron.*, vol. 16, no. 3, pp. 351–359, May 2001.

[3] T. Brückner and D. G. Holmes, "Optimal pulse-width for three-level inverters," *IEEE Trans. Power Electron.*, vol. 20, no. 1, pp. 82–89, Jan. 2005.

[4] B. P. McGrath, D. G. Holmes, and T. A. Lipo, "Optimized space vector switching sequences for multilevel inverters," *IEEE Trans. Power Electron.*, vol. 18, no. 6, pp. 1293–1301, Nov. 2003.

[5] O. Ojo, "The generalized discontinuous PWM scheme for three-phase voltage source inverters," *IEEE Trans. Industry Appl.*, vol. 51, no. 6, pp. 1280–1289, Nov./Dec. 2004.

[6] J. W. Kolar, H. Ertl, and F. C. Zach, "Influence of the modulation method on the conduction and switching losses of a PWM converter system," *IEEE Trans. Ind. Appl.*, no. 6, pp. 1063–1075, Nov./Dec. 1991.

[7] A. M. Trzynadlowski and S. Legowski, "Minimum-loss vector PWM strategy for three-phase inverters," *IEEE Trans. Power Electron.*, vol. 9, no. 1, pp. 26–34, Jan. 1994.

[8] D. Chung and S. Sul, "Minimum-loss strategy for three-phase PWM rectifier," *IEEE Trans. Ind. Electron.*, vol. 46, no. 3, pp. 517–526, 1999.

[9] M. Depenbrock, "Pulse width control of a three-phase inverter with nonsinusoidal phase voltages," in *Proc. ISPC Conf.*, 1977, pp. 399–403.

[10] A. M. Hava, R. J. Kerkman, and T. A. Lipo, "Carrier-based PWM-VSI overmodulation strategies: Analysis, comparison and design," *IEEE Trans. Power Electron.*, vol. 13, no. 4, pp. 674–689, Jul. 1998.

[11] L. Asiminoaei, P. Rodriguez, and F. Blaabjerg, "A new generalized discontinuous PWM strategy for active power filters," in *Proc. Applied Power Electronics Conf.*, 2007, pp. 315–321.

[12] J. W. Kolar, H. Ertl, and F. Zach, "Design and experimental investigation of a three-phase high power density PWM rectifier employing a novel semiconductor module," in *Proc. Applied Power Electronics Conf.*, 1996, vol. 2, pp. 514–523.

[13] O. Ojo and S. Konduru, "A discontinuous carrier-based PWM modulation method for the control of neutral point voltage of three-phase three-level diode clamped converters," in *Proc. Power Electron. Specialists Conf.*, 2005, vol. 2, pp. 1652–1658.

[14] N. Celanovic and D. Boroyevich, "A comprehensive study of neutral-point voltage balancing problem in three-level neutral-point-clamped voltage source PWM inverters," *IEEE Trans. Power Electron.*, vol. 15, no. 2, pp. 242–249, Mar. 2000.

[15] M. Marchesoni, P. Segarich, and E. Soressi, "A new control strategy for neutral-point-clamped active rectifiers," *IEEE Trans. Ind. Electron.*, vol. 52, no. 2, pp. 462–470, Apr. 2005.

[16] L. Dalessandro, U. Drofenik, S. D. Round, and J. W. Kolar, "A novel hysteresis current control for three-phase three-level rectifiers," in *Proc. Applied Power Electronics Conf.*, 2005, vol. 1, pp. 501–507.

[17] J. W. Kolar and U. Drofenik, "A new switching loss reduced discontinuous scheme for a unidirectional three-phase/switch/level boost-type PWM (Vienna) rectifier," in *Proc. Int. Telecommunication Energy Conf.*, 1999, pp. 490–499.

[18] F. Wang, "Sine-triangle versus space-vector modulation for three-level PWM voltage-source inverters," *IEEE Trans. Ind. Appl.*, vol. 38, no. 2, pp. 500–506, Mar./Apr. 2002.

[19] K. Zhou and D. Wang, "Relationship between space-vector modulation and three-phase carrier based PWM: A comprehensive analysis," *IEEE Trans. Ind. Electron.*, vol. 49, no. 1, pp. 186–196, Feb. 2002.

Luca Dalessandro (S'02–M'07) was born in Bari, Italy, on April 29, 1978. He received the M.Sc. degree (with first-class honors) from the Politecnico di Bari, Bari, Italy, in 2001 and the Ph.D. degree from the ETH Zurich, Swiss Federal Institute of Technology, Zurich, Switzerland, in 2007, both in electrical engineering.

From 2001 to 2002, he was a Researcher at the Max-Planck-Institute for Mathematics in the Sciences (MPI-MIS), Leipzig, Germany. From 2002 to 2006, he was a Research and Teaching Assistant at the Power Electronics Systems Laboratory (PES) of the ETH Zurich. In the summer of 2006, under a post-doctoral fellowship grant provided by the industry, he joined the National Science Foundation Engineering Research Center (NSF-ERC) for Power Electronics Systems (CPES), Virginia Polytechnic Institute and State University, Blacksburg. In the fall of 2006, he was appointed Adjunct Professor at the Bradley Department of Electrical and Computer Engineering, Virginia Tech. In 2007, he joined the Power Systems and High-Voltage Technology Institute (EEH) at ETH Zurich as a Research Associate. He has been an invited lecturer and visitor at several recognized institutions and companies, including the Massachusetts Institute of Technology (MIT), Cambridge, and the National Japanese Institute for Advanced Industrial Science and Technology (AIST), Japan. His research interests include all disciplines of electrical power engineering.

Dr. Dalessandro is the recipient of several awards and fellowships and is listed in *Who's Who in Science and Engineering*. He serves as an External Advisor the Swiss Embassy in Italy for international scientific events. He is a Registered Professional Engineer in Italy.

Simon Round (SM'01) received the B.E. (Hons.) and Ph.D. degrees from the University of Canterbury, Christchurch, New Zealand, in 1989 and 1993, respectively.

From 1992 to 1995, he was a Research Associate in the Department of Electrical Engineering, University of Minnesota and a Research Fellow at the Norwegian Institute of Technology, Trondheim, Norway. From 1995 to 2003, he was a Lecturer/Senior Lecturer in the Department of Electrical and Electronic Engineering, University of Canterbury, where he performed research on power quality compensators, electric vehicle electronics, and cryogenic power electronics. He was a Power Electronic Consultant for Vectek Electronics, where he developed a state-of-the-art digital controller for high-power inverter systems. In September 2004, he joined the Power Electronic Systems Laboratory at the Swiss Federal Institute of Technology (ETH), Zurich, Switzerland, as a Senior Researcher. His current research interests are in ultra-compact power converters, digital control, medium-voltage and high-temperature applications of silicon carbide power devices, and the application of sparse matrix converters. He has authored of over 75 publications in journals and international conferences.

Dr. Round has been actively involved in the IEEE New Zealand South Section, where he was Vice-Chair and Chairman from 2001 to 2004. He received a University of Canterbury Teaching Award in 2001.

Uwe Drofenik (S'96-M'00) was born in Moedling, Austria, in 1970. He received the M.Sc. (*cum laude*) and Ph.D. (*cum laude*) degrees in electrical engineering from the Vienna University of Technology, Vienna, Austria, in 1995 and 1999, respectively.

During 1996, he was a Visiting Researcher at the Masada-Ohsaki Laboratory at the University of Tokyo, Tokyo, Japan. From 1997 to 2000, he was a Scientific Assistant at Vienna University of Technology, where he was involved in power electronic projects and CAD/CAM software development. In 2001, he joined the Swiss Federal Institute of Technology (ETH), Zurich, Switzerland, as a Postdoctorate Researcher, where is heading the development of a multi-disciplinary simulation software for "Virtual Prototyping in Power Electronics", including programming and experimental testing of numerical circuit simulators, thermal and electromagnetic 3D-FEM simulators, algorithms for estimating reliability and lifetime of electronic components and systems, and the intelligent coupling of all these software-modules within a single design-platform. He is the author of the web-based interactive educational power-electronics software iPES. He has published more than 50 conference and journal papers and four patents.

Dr. Drofenik received the "Isao Takahashi Award" from the IEE Japan in 2005.

Johann W. Kolar (SM'04) received the Ph.D. degree (*summa cum laude/promotio sub auspiciis praesidentis rei publicae*) from the University of Technology Vienna, Vienna, Austria.

Since 1984, he has been an Independent International Consultant in close collaboration with the University of Technology Vienna in the fields of power electronics, industrial electronics, and high-performance drives. He has proposed numerous novel PWM converter topologies and modulation and control concepts, e.g., the VIENNA rectifier and the three-phase ac-ac sparse matrix converter. He was appointed Professor and Head of the Power Electronic Systems Laboratory, Swiss Federal Institute of Technology (ETH), Zurich, Switzerland, in February 2001. In 2006, the European Power Supplies Manufacturers Association (EPSMA) awarded the Power Electronics Systems Laboratory of ETH Zurich as the leading academic research institution in Europe. The focus of his current research is on ac-ac and ac-dc converter topologies with low effects on the mains, e.g., for power supply of telecommunication systems, More-Electric-Aircraft, and distributed power systems in connection with fuel cells. Further main areas of research are the realization of ultra-compact intelligent converter modules employing latest power semiconductor technology (SiC), novel concepts for cooling and EMI filtering, multidomain/multiscale modelling and simulation, pulsed power, bearingless motors, and Power MEMS. He has published over 250 scientific papers in international journals and conference proceedings and has filed more than 70 patents.

Dr. Kolar is a Member of the IEEJ and of the Technical Program Committees of numerous international conferences in the field (e.g., Director of the Power Quality Branch of the International Conference on Power Conversion and Intelligent Motion). From 1997 through 2000, he served as an Associate Editor of the IEEE TRANSACTIONS ON INDUSTRIAL ELECTRONICS and since 2001 as an Associate Editor of the IEEE TRANSACTIONS ON POWER ELECTRONICS. Since 2002, he has been an Associate Editor of the *Journal of Power Electronics* of the Korean Institute of Power Electronics and a member of the Editorial Advisory Board of the *IEEJ Transactions on Electrical and Electronic Engineering*. He received the Best Transactions Paper Award of the IEEE Industrial Electronics Society in 2005 and an Erskine Fellowship from the University of Canterbury, New Zealand, in 2003.